Available online at www.sciencedirect.com

SciVerse ScienceDirect

Ceramics International 39 (2013) 3771–3777

CERAMICS INTERNATIONAL

www.elsevier.com/locate/ceramint

Modified self-propagating high-temperature synthesis of nanosized $La_{0.7}Ca_{0.3}MnO_3$

Ana Mraković[a,*], Jovan Blanuša[a], Darinka Primc[b], Marija Perović[a], Zvonko Jagličić[c], Vladan Kusigerski[a], Vojislav Spasojević[a]

[a]The Vinca Institute, University of Belgrade, P. O. BOX 522, 11001 Belgrade, Serbia
[b]Jozef Stefan Institute, Department for Materials Synthesis, Jamova cesta 39, 1000 Ljubljana, Slovenia
[c]Institute of Mathematics, Physics and Mechanics, University of Ljubljana, Jadranska 19, 1000 Ljubljana, Slovenia

Received 4 September 2012; received in revised form 16 October 2012; accepted 17 October 2012
Available online 30 October 2012

Abstract

A modified solid-state combustion route was developed for the preparation of nanocrystalline manganite $La_{0.7}Ca_{0.3}MnO_3$ in a single-step process, using metal nitrates and glucose/KNO_3 redox mixture. The obtained sample was found to crystallize within O′ type of orthorhombic perovskite structure (space group *Pnma*), without the presence of other structural phases or impurities. Nanoparticles are found to have particle size in the range 12–35 nm, and to be highly crystalline without the presence of amorphous surface layer. Magnetic measurements show that nanoparticles display bulk-like magnetic properties, with ferromagnetic phase transition at 125 K and the absence of superparamagnetic or spin-glass behavior.

Keywords: B. X-ray methods; C. Magnetic properties; D. Perovskites; Combustion synthesis

1. Introduction

Doped rare earth manganites of the $La_{1-x}Ca_xMnO_3$ composition are subject of significant research interest during the last two decades due to their rich phase diagram and intriguing physical properties like colossal magneto-resistance (CMR), charge ordering (CO) or orbital ordering (OO) effects [1–3]. With research focus shifted to nanoparticle form, a number of synthesis methods for doped nanoparticle manganites are proposed and tested, including variety of wet chemistry, mechanochemistry and combustion methods [4–10]. Combustion synthesis or SHS (self-propagating high-temperature synthesis), is one of the preparation methods capable of meeting conflicting demands required in synthesis of nanoparticle mixed manganites (and nanoparticle solid solutions in general): the detention of small particle size, and simultaneously, the high synthesis temperature.

One version of SHS process, known as solution combustion (SC), is frequently used for synthesis of nanoparticle solid solutions [11,12]. It is based on a brief, exothermic burning reaction between oxidizing agent (usually the mixture of metal nitrates or acetates) and organic fuel (glycine, citric acid, urea, sucrose, etc.). By mixing of nitrates and fuel in a form of liquid solution, this approach provides the highest possible degree of precursor homogenization. Compared to many of the wet chemistry routes, SC method is advantageous since it is very simple to implement, it is time- and cost-efficient and it can easily provide large amounts of material [13–15]. This, however, is achieved at a cost of inability to retain precise control over particle size and morphology. Stochastic character of self-ignition and/or burning process often leads to inhomogeneous heat and temperature distribution through the reacting media. Consequently, the resulting product may not be single phase and the size distribution of obtained nanoparticles is broad. In addition, it is rarely possible to obtain samples by SC in a single step process [15,16], and the usual need for additional annealing at $T \geq 800$ °C often

*Corresponding author. Tel.: +381 11 80 65 828; fax: +381 11 80 65 829.
E-mail address: amrakovic@vinca.rs (A. Mraković).

0272-8842/$ - see front matter © 2012 Elsevier Ltd and Techna Group S.r.l. All rights reserved.
http://dx.doi.org/10.1016/j.ceramint.2012.10.216

hinders the possibility to obtain particles that are less than 30 nm in diameter.

SHS conducted in a solid state (SSC) represents another useful way to use combustion energy in synthesis of solid solutions [17,18]. In this approach, a mixture of reacting powders is pressed in cylindrical shape and ignited at one end, thus creating a heat wave that propagates (with well defined velocity) toward the other end of the cylinder. In SSC route, the burning reaction typically takes place between metal powder (as fuel) and the powders of metal oxides or nonmetallic elements (as oxidizers) [19]. However, with the combustion temperature commonly exceeding 2000 °C, this variation of SHS method was primarily developed for synthesis of polycrystalline ceramics that would be difficult to obtain by conventional sintering [17].

Application of standard SSC procedure in nanoparticle synthesis is limited both by its high temperature and by heterogeneity of powder mixture due to the micron-grade granular size. Nevertheless, better control over combustion process than in the case of SC synthesis represents an attractive motive for modification of SSC towards nanoparticle synthesis. Numerous attempts have been made in that direction, for example, through the reduction of temperature by adding rock salt to the mixture [20], or by subsequent high energy ball milling (HEBM) of polycrystalline products obtained under standard SSC procedure [21]. HEBM was also used to reduce the grain size of starting powders down to nanometric scale prior to combustion [21].

There were also attempts to replace the metal–metal oxide (thermite) type of reaction, in order to extend SSC applicability to a wider range of compounds, including manganites. For example, $NaClO_4$ was used as internal oxidizer of Mn metal during synthesis of polycrystalline mixed manganites [22], while the introduction of carbon as an internal fuel was reported in [23] for synthesis of submicron perovskite powders. Recently, Hwang et al. [24] have used aqueous solution of metal nitrates and organic fuel in the first phase of synthesis (as a part of typical SC procedure), but skipped self-ignition stage in liquid phase and conducted the combustion of the dried residue instead, to obtain nanoscale Ni–Zn ferrite powder.

In typical SC and SSC methods, metal salts or nonmetallic elements are simultaneously involved in two parallel processes; they serve both as fuel oxidizers and cation source for solid state reaction to form the final compound. While such concept may simplify the procedure, the need to maintain critical fuel/oxidizer ratio necessary for ideally balanced reaction makes the temperature and rate of combustion intrinsic to the choice of used compounds, with limited possibilities for additional control. Changes in fuel/oxidizer ratio can influence combustion dynamics to some extent, but can also lead to either unburned fuel residue or to incompletely formed product. Thus, it is reasonable to assume that keeping burning reaction (with a sole purpose of providing thermal energy) and the solid state reaction of metallic compounds as two simultaneous, albeit chemically independent processes, may offer more flexible control over the temperature and rate of solid state reaction.

In this work we propose the modification of SSC route, with the initial step in which both the internal oxidizer and organic fuel are added to the mixture of metal nitrates, all in the form of aqueous solution. The proposed modification has the main goal of setting up a simple, yet efficient and single step combustion process that will combine advantages of SC (good mixture homogenization) with those of SSC (better combustion control, higher degree of crystallinity). We demonstrate that this concept can be successfully applied to synthesis of nanoparticle $La_{0.7}Ca_{0.3}MnO_3$ (LCMO) mixed manganite.

2. Materials and methods

In the modified SHS route, appropriate amounts of reactants (glucose, KNO_3 and nitrates of La, Ca and Mn) are dissolved and mixed as an aqueous solution providing the maximum degree of homogenization as in the case of classical SC approach. After drying, solid mixture was burned in typical SSC manner to produce $La_{0.7}Ca_{0.3}MnO_3$ as the final product. The simple concept of this synthesis route is depicted in Fig. 1.

First, 1 M aqueous solutions of metal nitrates were mixed in the stoichiometric proportion according to manganite formula $La_{0.7}Ca_{0.3}MnO_3$. To this solution, aqueous solution of redox mixture—potassium nitrate (KNO_3) and glucose ($C_6H_{12}O_6$) was added. The overall number of moles of metal nitrates was 0.02, and the molar ratio between metal nitrates/glucose/KNO_3 was 1.01/0.28/1. The final solution was

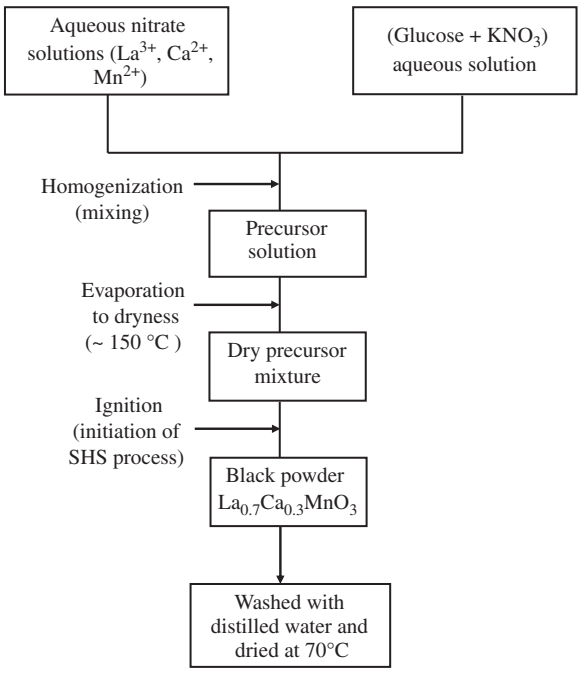

Fig. 1. Flow chart for combustion synthesis of $La_{0.7}Ca_{0.3}MnO_3$ nanopowder.

evaporated on a hot plate (150–170) °C until the formation of brown paste-like mass. This dried precursor was formed into a cylindrical shape while warm (0.5 cm in diameter, 4 cm long), and ignited in normal atmospheric conditions (room temperature, air). The ignition was initiated locally at one end of the cylinder by means of an open flame, launching a self-sustaining reaction which propagates with constant velocity ($\approx$ 1 cm/min), leaving the product in the form of black, fluffy powder behind the thin (about 1 mm thick) combustion zone. Since initial XRD observations of as-prepared powder revealed traces of K_2CO_3 residue, the product was washed several times with distilled water and dried at 70 °C.

The structural analysis of the final specimen was performed by X-ray diffraction on a Philips PW-1710 diffractometer at room temperature with CuKα radiation. The pattern was recorded in the 10°–100° 2θ range with the step size 0.05° and exposure time of 15 s/step. Structural parameters were refined by the Rietveld full-profile analysis method with the application of the FULLPROF software package.

High resolution transmission electron microscopy (HRTEM) has been used for particle size and morphology characterization of the obtained sample by JEM-2010F microscope operating at 200 keV. For the HRTEM investigations, the particles were milled in mortar and dispersed in acetone. The suspended particles were deposited on a copper-grid-supported perforated transparent carbon foil.

The magnetic characterization of the sample was done by utilizing superconducting quantum interference device magnetometer (Quantum Design MPMS XL-5) in the temperature range 2–300 K and applied fields up to 50 kOe.

3. Results and discussion

3.1. Transmission electron microscopy and X-ray diffraction

The TEM image (Fig. 2a) shows the LCMO sample which is composed of agglomerated globular to round-cornered cuboid particles, while the corresponding electron diffraction pattern (Fig. 2b) is indexed according to orthorhombic structure of $(La_{0.66}Ca_{0.33})MnO_3$ (JCPDS no. 87-1084). The size distribution of nanoparticle LCMO was measured directly from raw TEM micrographs, and the average particle size (equivalent diameter) was estimated to be $d=(22\pm6)$ nm. It can be seen from the corresponding histogram (shown in Fig. 3), that particle size varies from 12 nm to 35 nm. Since 90% of particles are distributed between 16 nm and 28 nm, this can be considered as a relatively narrow distribution for the sample obtained by combustion synthesis, especially considering that no additional thermal treatment was applied.

The HRTEM image of one round-cornered cuboid particle (Fig. 2d) shows that the lattice image is terminated at the surface of the particles, revealing no amorphous

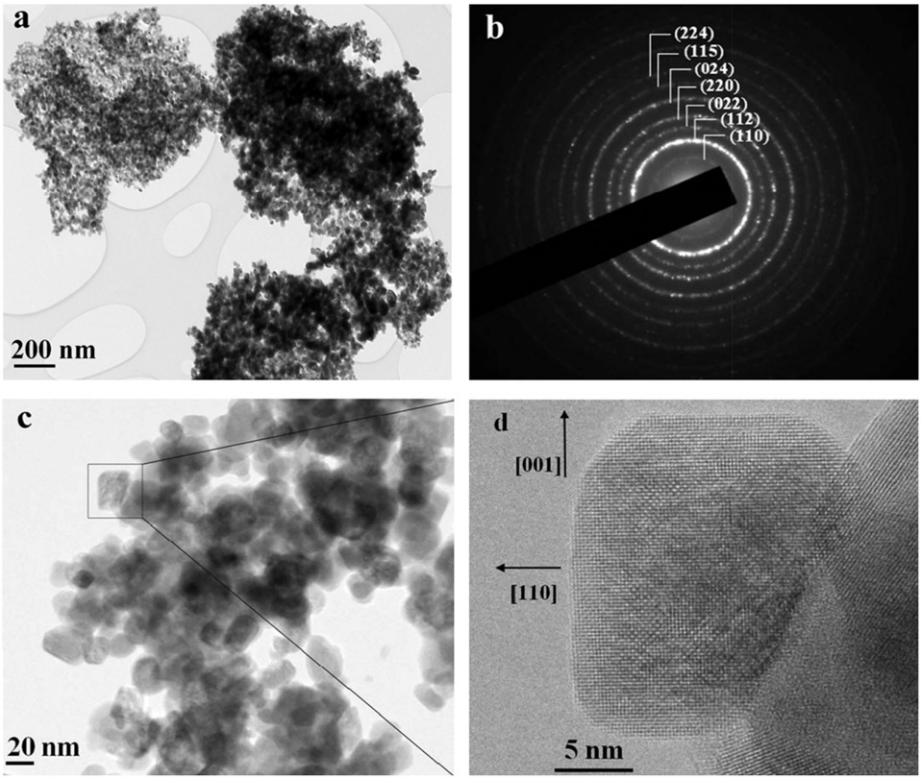

Fig. 2. (a) Representative TEM image of the sample $La_{0.7}Ca_{0.3}MnO_3$; (b) diffraction pattern of the same sample area; (c) part of the sample under increased magnification; and (d) HRTEM micrograph reveals the absence of the amorphous layer on the particles surface.

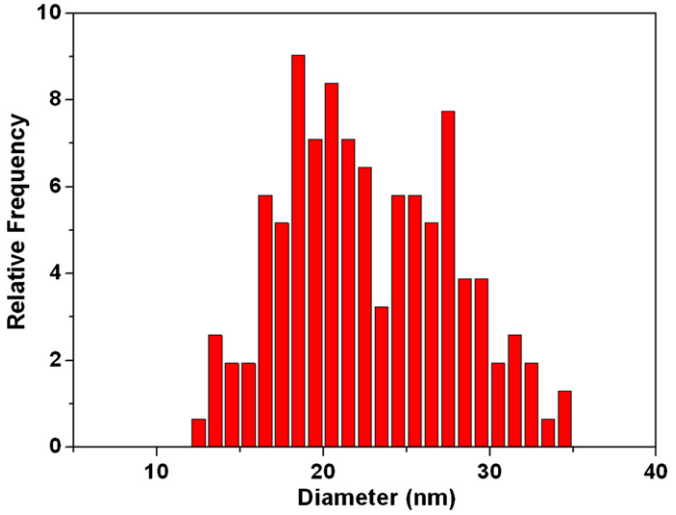

Fig. 3. The histogram shows the size distribution of the equivalent diameters for the LCMO nanoparticles measured from TEM micrographs.

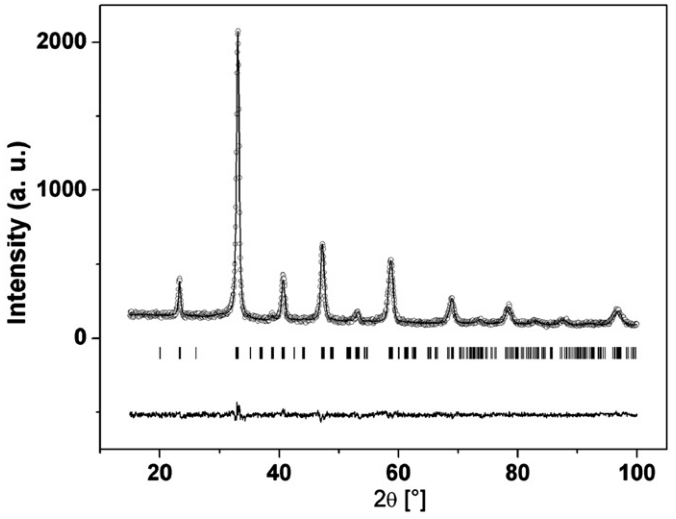

Fig. 4. The X-ray pattern (open symbols) and Rietveld fit (line) for LCMO. The curve at the bottom is the difference between the observed and calculated intensities while vertical bars indicate the positions of the Bragg reflections for orthorhombic LCMO structure.

layer on the surface. Thus, despite the small particle size, both image observation and electron diffraction pattern point to highly crystallized nanoparticles.

The X-ray diffraction pattern of the LCMO sample, refined by full-profile Rietveld method, is shown in Fig. 4. The applied analysis included structure and microstructure (particle size and strain) characterization, using TCH (Thompson–Cox–Hastings) approximation of Voigt function to describe the profile of XRD lines [25]. Instrumental line broadening has been determined using CeO_2 powder as standard.

The results of refinement confirmed that the sample crystallized as single phase, without presence of impurities or other structural phases. It should be noted that neither XRD diffraction, nor magnetic measurements (presented in Section 3.2.), did not reveal traces of Mn_3O_4, the most frequent impurity accompanying nanoparticle combustion synthesis in normal atmospheric conditions. Since Mn_3O_4 impurity in manganites is regularly eliminated by annealing in oxygen rich atmosphere, its absence in our sample can be explained by the local oxygen excess present due to the decomposition of metal nitrates.

Within the Rietveld refinement procedure, the best agreement with experimental diffraction pattern was found for structure model comprising orthorhombic *Pnma* space group (No. 62) and the asymmetric unit shown in Table 1. The lattice parameters $a=5.45348$ (55) Å, $b=7.70490$ (73) Å and $c=5.50525$ (53) Å, fulfill the condition of $c/a<\sqrt{2}$, thus the observed orthorhombic distortion is of O′ type in respect to ideal cubic perovskite structure [26]. The refinement of the structure converged with Bragg profile and integral factors $R_{wp}=16.1\%$ and $R_B=4.06\%$, respectively.

It is important to note that the relative intensity of diffraction peaks was not possible to refine properly unless ~7.5% of total Mn content is relocated from its standard 4b site into another site with the same local symmetry, 4a (Table 1). This result may be the consequence of abrupt temperature drop behind relatively thin combustion zone, due to the large amount of liberated gases which acts as an efficient heat sink, leading to the "quenching" of the LCMO nanocrystals structure.

Since no significant particle shape anisotropy (needle or platelet) was found by TEM analysis, the spherical harmonics modeling [27] was applied within size/strain analysis in the Rietveld refinement. The values obtained for average crystallite diameter and microstrain were 219.9(0.2) Å and $35.53(0.06)\times10^{-4}$, respectively. The average particle size of 22 nm is in a very good agreement with TEM observations. However, somewhat higher strain value does not reflect the high degree of crystallinity found by HRTEM analysis, which can be linked to the partial Mn disorder between 4a and 4b sites within the unit cell.

3.2. Magnetic properties

The magnetic analysis of LCMO sample shows an interesting mixture of bulk- and nano-characteristics, originating from the combination of high crystallization degree and small particle size. Some of LCMO magnetic properties resemble behavior that is typical of nanoparticle manganites such as: reduction of magnetic phase transition temperature, the broad maximum in ZFC magnetization (Fig. 5), and the absence of full saturation in hysteresis loops up to 5 T (Fig. 7). The ferromagnetic phase transition temperature (T_C) was determined as the minimum in the derivative of the FC magnetization curve and is found to be ~125 K, which is considerably reduced in comparison with 280 K reported for the bulk counterpart of the same composition [28]. On the other hand, no superparamagnetic or spin-glass like behavior were detected in this sample by magnetic measurements.

Table 1
Refined atom positions of orthorhombic $La_{0.7}Ca_{0.3}MnO_3$ (space group *Pnma*).

Atom	Position	*x* (Å)	*y* (Å)	*z* (Å)	Atomic occupation
La	**4(c)**	−0.00747(81)	0.25	0.99764(218)	2.8
Ca	**4(c)**	−0.00747(81)	0.25	0.99764(218)	1.2
Mn	**4(b)**	0	0	0.5	3.65(6)
Mn	**4(*a*)**	0	0	0	0.35(6)
O(1)	**4(c)**	0.50375(349)	0.25	0.08813(71)	4.0
O(2)	**8(d)**	0.21054(456)	0.02104(397)	0.75100(663)	8.0

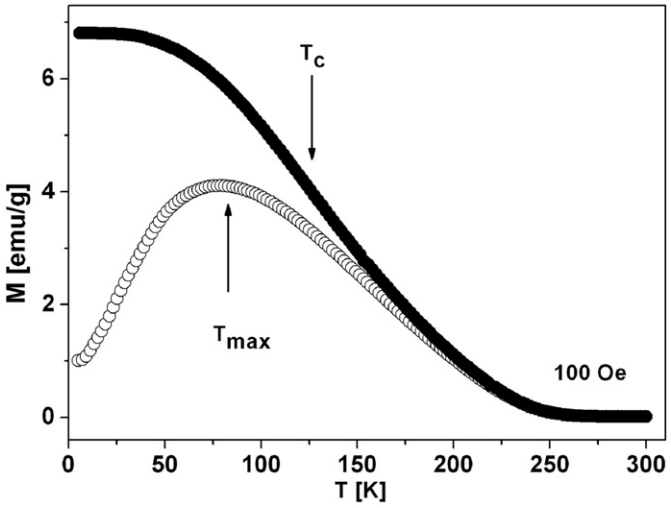

Fig. 5. Temperature dependence of ZFC (open symbols) and FC (solid symbols) magnetization of LCMO sample measured in $H=100$ Oe.

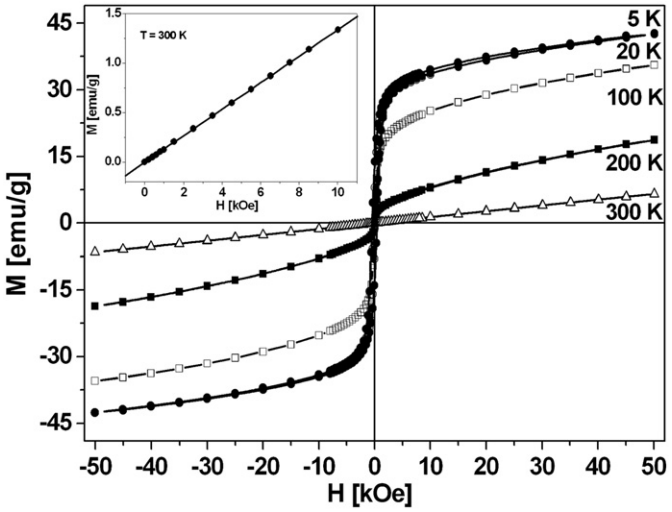

Fig. 7. Hysteresis loops of LCMO sample recorded at 5 K, 20 K, 100 K, 200 K and 300 K. The inset shows M versus H dependence in field up to 1 T at $T=300$ K; full line represents linear fit to the Eq. (1).

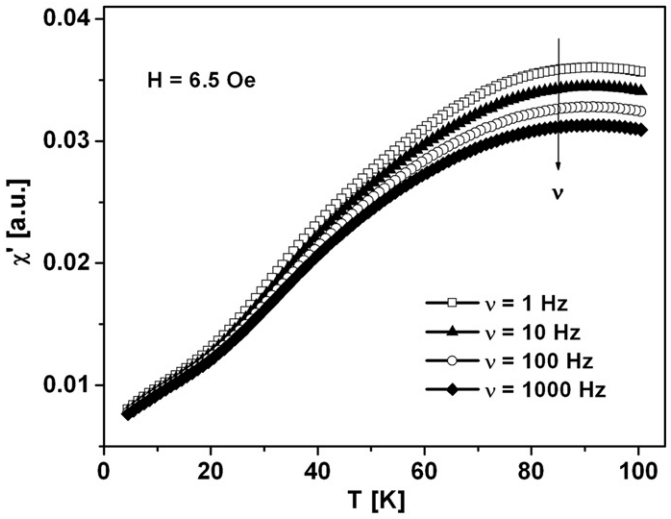

Fig. 6. Temperature dependence of the real part of the AC susceptibility at different frequencies, measured in the temperature region 5–100 K.

The value of the effective magnetic moment of Mn ion obtained from the Curie–Weiss law within 250–300 K temperature range is $\mu_{eff}=(4.7\pm0.1)\,\mu_B$, which is in a good agreement with theoretical value of 4.62 μ_B corresponding to the stoichiometric mixture of 70% Mn^{3+} (4.9 μ_B) and 30% Mn^{4+} (3.87 μ_B), calculated by $\mu_{eff}^2=0.7\mu^2(Mn^{3+})+0.3\mu^2(Mn^{4+})$. This, in addition to results of XRD analysis, confirms correct La/Ca ratio and the proper oxygen content in the sample. However, the used temperature interval was not sufficiently wide for accurate determination of Curie–Weiss temperature Θ, which was estimated more accurately by using linear part of $M(H)$ dependence at 300 K, in the field range of 0–1 T (Fig. 7):

$$M=\frac{C}{T-\Theta}H \tag{1}$$

By assuming 4.7 μ_B for the value of effective magnetic moment, the obtained Θ value was found large and positive (202 ± 1) K, which is lower than bulk value of 275 K [28], but still confirms the presence of strong ferromagnetic interaction in nanoparticle sample.

FC magnetization continuously increases with decreasing temperature, while ZFC magnetization displays pronounced maximum at temperature $T_{max}\sim80$ K (Fig. 5), which indicates gradual blocking/freezing of nanoparticle magnetic moments. On the other hand, FC magnetization below T_{max} tends to saturate. This flatness of FC magnetization at low temperatures and particle agglomeration

observed in TEM micrographs, point to a certain degree of inter-particle interactions.

In order to further investigate the nature of ZFC maximum, ac susceptibility measurements were carried out. The temperature dependence of the real part χ' (T) of ac magnetic susceptibility measured at several frequencies in the 1–1000 Hz range and an ac field amplitude of 6.5 Oe is shown in Fig. 6. χ' (T) exhibits a peak at the temperature $T\sim 91$ K, which position does not shift with frequency, while only the peak intensity slightly decreases with v. Similar trend in experimentally obtained AC curves was also reported for nanoparticle sample of the same composition [29], which was obtained by SC (glycine–nitrate) method and subsequently annealed at 900 °C. This type of behavior in magnetic nanoparticles can be attributed to the bulk-like nature of the investigated sample, and strongly depends upon the crystal quality of the sample [30]. Since TEM micrographs showed that our LCMO nanoparticles are highly crystalline with absence of amorphous layer on the particle surface, bulk-like magnetic behavior is expected.

4. Conclusions

In summary, this paper presents the novel route for solid state SHS synthesis of nanoparticle materials, which is successfully applied for the preparation of 20 nm LCMO nanoparticles. We have demonstrated that, by using this approach to combustion synthesis, it is possible to obtain pure, well-crystallized nanoparticles in a single-step combustion process, without requirement for additional thermal treatment. Contrary to most combustion methods, proposed SHS route enables synthesis of nanoparticle LCMO in a relatively narrow size distribution and free from distorted surface ("shell") layer, thus minimizing surface effects and promoting bulk-like magnetic behavior.

Due to the separation of combustion process from solid state reaction between metal oxides, combustion method applied in this work offers wide possibilities for adjustments of reaction temperature and rate, since the ratio between redox mixture (glucose + KNO_3) and metal salts is freely adjustable. Another advantage that deserves attention in further studies is that, by the choice of used metal salts or by the addition of independent oxidizing or reducing agents, such approach offers the possibility to regulate local oxido–reductive atmospheric conditions during reaction.

Acknowledgments

This project was financially supported by the Ministry of Education and Science, Republic of Serbia (Project no. III 45015).

References

[1] E.L. Nagaev, Colossal-magnetoresistance materials: manganites and conventional ferromagnetic semiconductors, Physics Reports 346 (2001) 387–531.

[2] M.B. Salamon, The physics of manganites: structure and transport, Reviews of Modern Physics 73 (2001) 583–628.

[3] C.N.R. Rao, Charge, spin, and orbital ordering in the perovskite manganates, $Ln_{1-x}A_xMnO_3$ (Ln = rare earth, A = Ca or Sr), Journal of Physical Chemistry B 104 (2000) 5877–5889.

[4] K.S. Shankar, A.K. Raychaudhuri, Low-temperature polymer precursor-based synthesis of nanocrystalline particles of lanthanum calcium manganese oxide ($La_{0.67}Ca_{0.33}MnO_3$) with enhanced ferromagnetic transition temperature, Journal of Materials Research 21 (2006) 27–33.

[5] S.M. Zhou, S.Y. Zhao, L.F. He, Y.Q. Guo, L. Shi, Facile synthesis of Ca-doped manganite nanoparticles by a nonaqueous sol–gel method and their magnetic properties, Materials Chemistry and Physics 120 (2010) 75–78.

[6] T. Ahmad, K.V. Ramanujachary, S.E. Lofland, A.K. Ganguli, Reverse micellar synthesis and properties of nanocrystalline GMR materials ($LaMnO_3$, $La_{0.67}Sr_{0.33}MnO_3$, $La_{0.67}Ca_{0.33}MnO_3$): ramifications of size considerations, Journal of Chemical Sciences 118 (2006) 513–518.

[7] A.M. Boların, F. Sanchez, S. Palomares, J.A. Aguilar, G. Torres-Villasenor, Synthesis of calcium doped lanthanum manganite by mechanosynthesis, Journal of Alloys and Compounds 436 (2007) 335–340.

[8] B.M. Nagabhushana, R.P. Sreekanth Chakradhar, K.P. Ramesh, C. Shivakumara, G.T. Chandrappa, Combustion synthesis, characterization and metal–insulator transition studies of nanocrystalline $La_{1-x}Ca_xMnO_3$ ($0.0 \le x \le 0.5$), Materials Chemistry and Physics 102 (2007) 47–52.

[9] L. da Conceicao, N.F.P. Ribeiro, J.G.M. Furtado, M.M.V.M. Souza, Effect of propellant on the combustion synthesized Sr-doped $LaMnO_3$ powders, Ceramics International 35 (2009) 1683–1687.

[10] R. Epherre, E. Duguet, S. Mornet, E. Pollert, S. Louguet, S. Lecommandoux, C. Schatz, G. Goglio, Manganite perovskite nanoparticles for self-controlled magnetic fluid hyperthermia: about the suitability of an aqueous combustion synthesis route, Journal of Materials Chemistry 21 (2011) 4393–4401.

[11] K.C. Patil, S.T. Aruna, T. Mimani, Combustion synthesis: an update, Current Opinion in Solid State and Materials Science 6 (2002) 507–512.

[12] S.T. Aruna, A.S. Mukasyan, Combustion synthesis and nanomaterials, Current Opinion in Solid State and Materials Science 12 (2008) 44–50.

[13] K. Prabhakaran, J. Joseph, N.M. Gokhale, S.C. Sharma, R. Lal, Sucrose combustion synthesis of $La_xSr_{(1-x)}MnO_3$ ($x \le 0.2$) powders, Ceramics International 31 (2005) 327–331.

[14] E. Magnone, E. Traversa, M. Miyayama, Nano-sized $Pr_{0.8}Sr_{0.2}Co_{1-x}Fe_xO_3$ powders prepared by single-step combustion synthesis for solid oxide fuel cell cathodes, Journal of Electroceramics 24 (2010) 122–135.

[15] C.M. Fu, M.R. Syue, F.J. Wei, C.W. Cheng, C.S. Chou, Synthesis of nanocrystalline Ni–Zn ferrites by combustion method with no post-annealing route, Journal of Applied Physics 107 (2010) 1–3 09A519.

[16] D. Markovic, V. Kusigerski, M. Tadic, J. Blanusa, M.V. Antisari, V. Spasojevic, Magnetic properties of nanoparticle $La_{0.7}Ca_{0.3}MnO_3$ prepared by glycine-nitrate method without additional heat treatment, Scripta Materialia 59 (2008) 35–38.

[17] A.G. Merzhanov, The chemistry of self-propagating high-temperature synthesis, Journal of Materials Chemistry 14 (2004) 1779–1786.

[18] A.G. Merzhanov, I.P. Borovinskaya, Historical Retrospective of SHS: an autoreview, International Journal of Self-Propagating High-Temperature Synthesis 17 (2008) 242–265.

[19] K.C. Patil, S.T. Aruna, S. Ekambaram, Combustion synthesis, Current Opinion in Solid State and Materials Science 2 (1997) 158–165.

[20] H.H. Nersisyan, J.H. Lee, C.W. Won, The synthesis of nanostructured molybdenum under self-propagating high-temperature synthesis mode, Materials Chemistry and Physics 89 (2005) 283–288.

[21] T. Grigorieva, M. Korchagin, N. Lyakhov, Combination of SHS and mechanochemical synthesis for nanopowder technologies, Kona 20 (2002) 144–158.

[22] M.V. Kuznetsov, I.P. Parkin, D.J. Caruanab, Y.G. Morozov, Combustion synthesis of alkaline-earth substituted lanthanum manganites;

$LaMnO_3$, $La_{0.6}Ca_{0.4}MnO_3$ and $La_{0.6}Sr_{0.4}MnO_3$, Journal of Materials Chemistry 14 (2004) 1377–1382.

[23] K.S. Martirosyan, M. Iliev, D. Luss, Carbon combustion synthesis of nanostructured perovskites, International Journal of Self-Propagating High-Temperature Synthesis 16 (2007) 36–45.

[24] C.C. Hwang, T.Y. Wu, J. Wan, Design and modify the combustion synthesis method to synthesize ceramic oxide powders, Journal of Materials Science 39 (2004) 4687–4691.

[25] P. Thompson, D.E. Cox, J.B. Hastings, Rietveld refinement of Debye–Scherrer synchrotron X-ray data from Al_2O_3, Journal of Applied Crystallography 20 (1987) 79–83.

[26] L. Malavasi, M.C. Mozzati, P. Ghigna, G. Chiodelli, C.B. Azzoni, G. Flor, Role of point defects on the properties of manganites, unpublished results, 2004 〈http://arXiv:cond-mat/0412606v1〉.

[27] Juan Rodríguez-Carvajal, Fullprof program manual 〈http://diffraction.web.psi.ch/pdf/fullprof-manual.pdf〉, 2001.

[28] R.N. Bhowmik, A. Poddar, R. Ranganathan, C. Mazumdar, Magnetism of crystalline and amorphous $La_{0.67}Ca_{0.33}MnO_3$ nanoparticles, Journal of Applied Physics 105 (113909) (2009) 1–11.

[29] D. Markovic, V. Kusigerski, M. Tadic, J. Blanusa, Z. Jaglicic, N. Cvjeticanin, V. Spasojevic, The influence of the heat treatment on the structural and magnetic properties of nanoparticle $La_{0.7}Ca_{0.3}MnO_3$ prepared by glycine–nitrate method, Journal of Alloys and Compounds 494 (2010) 52–57.

[30] X. Batlle, N. Pérez, P. Guardia, O. Iglesias, A. Labarta, Magnetic nanoparticles with bulk-like properties, Journal of Applied Physics 109 (2011) 1–6 07B524.